Comput Visual Sci (2009) 12:101–114
DOI 10.1007/s00791-008-0084-2

REGULAR ARTICLE

Mumford–Shah based registration: a comparison of a level set and a phase field approach

Marc Droske · Wolfgang Ring · Martin Rumpf

Received: 13 August 2005 / Accepted: 13 January 2006 / Published online: 29 January 2008

Abstract Traditionally, different image processing tasks are mainly considered on their own. The main aim of this paper is a combination of *registration*, i.e., the spatial alignment of images and *segmentation*, i.e., the recognition of edges and object contours in images. A proper registration depends on a good initial segmentation and vice versa. In this paper, it is proposed to link these problems together by formulating a coupled variational problem. We will focus on an edge-based approach instead of considering image intensities and propose a variational formulation based on the Mumford–Shah free discontinuity problem. This paper is particularly devoted to a comparison of a sharp interface approach with the phase field analogue.

1 Introduction

Especially on the background of medical applications denoising, segmentation and registration are well established as fundamental problems in image processing. An enormous amount of state-of-the-art imaging methods enables precise studies of the immense *variability* of human anatomy. We refer to the reviews by Miller et al. [55], the overview article of Grenander and Miller [43] and [46,57] for numerical aspects. Frequently, different images show corresponding structures at usually nonlinearly transformed positions [50,56,67]. As the image modality differs there is also no correlation of image intensities at corresponding positions. But an at least partial correspondence of edge sets is feasible. Hence, edge segmentation might help in the registration. On the other hand, integrated knowledge from different image modalities will lead to better segmentation. This circular dependence of registration and edge segmentation is well-known. One might think for example of a pair *magnetic resonance* (MR) and *computed tomography* (CT) images, or simply a color image instead of a gray scale image. An alternative, global morphological matching approach has been presented by Viola and Wells [71], Wells et al. [73] and Collignon et al. [53] based on a information theoretic approach for the registration of multi-modal images. Their information theoretic method is based on a maximization of the so called mutual information of images of different modality. In [38] a variational approach not relying on statistics is proposed for morphological matching. Both approaches do not make explicit use of segmentation results.

Here, we focus on the registration of edges. The set of detectable edges in the different images or color channels is often disrupted and irregular. Furthermore, they are most often given by binary indicators, hence information about *weak* edges is destroyed and often neglected. Let us first assume that we enrich the image space by overlaying several images, which have been registered perfectly in a preprocessing step. Features which are very weak and hardly visible in one of the images might be clear and salient in the other image. A feature detection model may now exploit the complementary information of both images

On the other hand, if a reliable segmentation of important objects in two images is available, the process of registra-

Communicated by K. Mikula.

M. Droske (✉) · M. Rumpf
Institute for Numerical Simulation, University of Bonn,
Nussallee 15, 53115 Bonn, Germany
e-mail: marc.droske@ins.uni-bonn.de

M. Rumpf
e-mail: martin.rumpf@ins.uni-bonn.de

W. Ring
Institute of Mathematics, University of Graz,
Heinrichstr. 36, Room 427, 8010 Graz, Austria
e-mail: wolfgang.ring@kfunigraz.ac.at

tion can be aided significantly. Mapping the object contours in the reference onto the contours in the template image, significantly simplifies the search space. The deformation is already determined on these boundaries modulo tangential distortion.

Due to this dependency it appears natural to combine both problems into one model. From a more general point of view, this would correspond to a simultaneous detection of image features, that ought to be coupled by a deformation. The subtlety of this approach is that edge contours as well as the deformation are unknowns. The whole process can be described as follows:

Given a pair of images, a reference and a template image, we aim to find a deformation and, simultaneously, a set of edges in the reference image, such that the transformed edge set matches the edges in the template image. Furthermore, the deformation itself and the edge sets should be regular.

In this formulation, the deformation is initially only determined on the set itself. Eventually we aim at a smooth extension of this deformation to the rest of the image domain in order to obtain a mapping of the images also away from the feature sets. We are going to ensure smoothness of the deformation and smoothness of the deformed edge set incorporating an elastic variational model for the deformation.

To motivate our approach let us first briefly review the variational approach presented by Mumford and Shah [59] and thereby describe in more mathematical detail what is meant by feature extraction and regularity of the edge set.

Mumford and Shah proposed to consider the following functional

$$E_{\mathrm{MS}}[u,\Gamma] = \int_{\Omega} (u-u_0)^2 \mathrm{d}x + \frac{\mu}{2}\int_{\Omega\setminus\Gamma} \|\nabla u\|^2 \,\mathrm{d}x + \nu\mathscr{H}^{d-1}(\Gamma). \tag{1}$$

The mathematical treatment of this energy is subtle. It has to be minimized over the set of admissible curves Γ and admissible u simultaneously. However, it is not possible to obtain lower-semicontinuity of the Hausdorff measure within a reasonable topology of subsets of Ω.

The existence theory is established by De Giorgi et al. [32] who proposed to consider the minimization of the energy depending on u only, and the set of admissible functions is chosen as $\mathrm{SBV}(\Omega)$, the space of functions of bounded variation u for which the measure Du can be written as $Du = \nabla u\lambda + (u^+ - u^-)n\mathscr{H}^{d-1}|S(u)$, i. e., the *Cantor* part of the support of the singular part of the measure known from BV functions is empty [3]. Here, u^+ and u^- denote the approximate lim sup resp. lim inf of u. The edge set Γ is now represented by S_u the complement set of Lebesgue points of u, i. e., the measure theoretic discontinuity set of u. Using the compactness of $\mathrm{SBV}(\Omega)$ (cf. Ambrosio et al. [3], [39]) and corresponding lower-semicontinuity results, one proves under mild assumptions that there exists a solution $u \in SBV(\Omega)$ with $\mathcal{H}^{d-1}(S_u) < \infty$. Especially due to the complexity of discretizing the singularity set, various approximations E_ϵ of the Mumford–Shah functional have been introduced for which Γ-convergence results are known (cf. e.g. [4,5,8,63]). We also refer to [1,13,26,28,42,68] for related topics and further extensions based on the Mumford–Shah functional.

Now, given different images with non aligned edges we can formulate a Mumford Shah type approach for both images with the constraint that the edge set in one images is given as the deformed edge set of the other image, where the deformation is controlled by an additional non linear elastic energy. To ensure that this deformation is one-to-one we consider a polyconvex elastic functional (cf. the work of Ball [6] and the overview given in [23,29]):

$$E_{\mathrm{reg}}[\phi] = \int_{\Omega} \hat{W}(D\phi, \mathrm{Cof}\, D\phi, \det D\phi)\,\mathrm{d}x, \tag{2}$$

where $\hat{W}$ is convex and $\hat{W} \to \infty$ for $\det D\phi \to 0, +\infty$.

This overall concept has been worked out in [36] for a level set formulation and in the thesis of one of the authors [35], where in addition to the level set formulation the phase field approach is already presented. In [37] the phase field model for edge registration is combined with the morphological matching approach—first presented in [38]—to achieve a matching of the regular as well as singular image morphologies. In this paper, our focus is on the comparison of the level set and the phase field approach for the simultaneous segmentation and matching of edge sets.

Let us point out, that the free discontinuity based approach proposed here is only a template study which fits into the general formulation of the joint feature extraction and registration problem. Different classes of images may require different models to drive the contour Γ towards the significant features of the images, e.g., a geodesic active contour model as proposed by Caselles et al. [18]. Yezzi et al. [51] have shown results for the coupling of the geodesic contour model and registration (see also the related work on subjective surfaces by Mikula et al. [54]) which would lead to a coupled energy of the form

$$E_{\mathrm{ac}}[\Gamma,\boldsymbol{\phi}] = \int_{\Gamma} g_R\,\mathrm{d}a + \nu\int_{\Omega} g_R\mathrm{d}x + \int_{\Gamma^\phi} g_T\,\mathrm{d}a + \nu\int_{\Omega} g_T\mathrm{d}x, \tag{3}$$

where g_R and g_T correspond to some suitable edge detectors in the images u_R and u_T. A common choice is, for example, $g_u(x) = (1 + s|\nabla u(x)|^2)^{-1}$, $s > 0$ (see [47] for a Newton-Type algorithm of the geodesic contour model). A related algorithm is described by Unal et al. [69], taking into account a joint energy for contour curves in different images. Féron and Mohammad-Djafari [41] proposed a Bayesian approach for the joint segmentation and fusion of images via a coupling of suitable hidden Markov Models for multi modal images. Vemuri et al. [70] have used a level set technique to exploit a reference segmentation in an atlas. We refer to [31] for further ideas.

2 A coupled Mumford–Shah model

By minimizing the Mumford–Shah functional we will obtain an approximation of the discontinuity sets of a noisy initial image u_0. Now, we consider a template image u_T and a reference image u_R at the same time. Furthermore, we ask for a deformation ϕ, which ensures that the discontinuity set $S[u_{R,0}]$ will be mapped onto the discontinuity set of u_T, i. e., $\phi(S[u_{R,0}]) = S[u_{T,0}]$. This can be achieved considered the following functional [36]:

$$\begin{aligned}\tilde{E}_{\mathrm{MS}}[\Gamma, \boldsymbol{\phi}, u_R, u_T] = &\frac{1}{2}\int_{\Omega}(u_R - u_{R,0})^2\,\mathrm{d}x \\ &+ \frac{\mu}{2}\int_{\Omega\setminus\Gamma}\|\nabla u_R\|^2\,\mathrm{d}x + \nu\mathscr{H}^{d-1}(\Gamma) \\ &+ \frac{1}{2}\int_{\Omega}(u_T - u_{T,0})^2\,\mathrm{d}x \\ &+ \frac{\mu}{2}\int_{\Omega\setminus\Gamma^{\boldsymbol{\phi}}}\|\nabla u_T\|^2\,\mathrm{d}x + \nu\mathscr{H}^{d-1}(\Gamma^{\boldsymbol{\phi}}).\end{aligned}$$

Here $\Omega \subset \mathbb{R}^d$ is the domain of definition of the images with $d = 2, 3$, $u_{T,0}, u_{R,0} \in L^\infty(\Omega)$ are the given initial template and reference images, $\Gamma \subset \Omega$ is (an approximation of) the edge set of the given image $u_{R,0}$ and $\Gamma^{\boldsymbol{\phi}} = \boldsymbol{\phi}(\Gamma)$ is the transformed edge-set Γ under the transformation $\boldsymbol{\phi}$.

The first line in the integral represents the usual Mumford–Shah segmentation model for the reference image $u_{R,0}$, while the second line adapts the same model for the template image $u_{T,0}$, but with an edge set given as the image of the edge set in the reference image under the deformation ϕ. Clearly, if u_T and u_R are minimizers of the original Mumford–Shah functional and $\boldsymbol{\phi}$ is chosen such that $\Gamma^{\boldsymbol{\phi}} = S(u_T)$ this energy is minimal. We see, that the deformation is obviously not uniquely determined by this condition, not even on the edge set itself, since reparametrization along the edge set does not change the energy. Furthermore, the energy does not consider the behavior of $\boldsymbol{\phi}$ away from the edge set. As proposed above, we add the nonlinear elastic energy $\alpha E_{\mathrm{reg}}[\phi]$ (2), which is supposed to control the regularity of the deformation ϕ and suitably extends deformations onto $\Omega\setminus\Gamma$. In order to avoid technical difficulties we avoid the length-measurement of Γ^ϕ and solely measure the length of Γ. Thus, length of Γ^ϕ is only implicitly controlled by the length of Γ and the regularity of ϕ. Finally, we end up with the following variational model

$$E[\Gamma, \phi, u_R, u_T] = E_{\mathrm{MS}}[\Gamma, \phi, u_R, u_T] + \alpha E_{\mathrm{reg}}[\phi], \tag{4}$$

where

$$\begin{aligned}E_{\mathrm{MS}}[\Gamma, \boldsymbol{\phi}, u_R, u_T] = &\frac{1}{2}\int_{\Omega}(u_R - u_{R,0})^2\,\mathrm{d}x \\ &+ \frac{\mu}{2}\int_{\Omega\setminus\Gamma}\|\nabla u_R\|^2\,\mathrm{d}x + \nu\mathscr{H}^{d-1}(\Gamma) \\ &+ \frac{1}{2}\int_{\Omega}(u_T - u_{T,0})^2\,\mathrm{d}x \\ &+ \frac{\mu}{2}\int_{\Omega\setminus\Gamma^{\boldsymbol{\phi}}}\|\nabla u_T\|^2\,\mathrm{d}x.\end{aligned} \tag{5}$$

3 A level set approach

In this section, we will review a level set model for the coupled free discontinuity problem (4). Thereby, we restrict ourselves to edge sets which are the union of finitely many Jordan-curves. In this case, the feature set can be viewed as the boundary of detected segments, which are mapped to similar segment boundaries in the second image. For a large class of images, this is a very suitable and convenient approach, since images can often be decomposed into a finite set of independent objects. However this is not always the case. Crack tips might occur not only due to weak edge information but due to the fact that the image contains disrupted discontinuity sets (cf. the phase field approximation below).

In a shape optimization framework [14,15], we start with an initial shape describing the edge set and evolve it based on a suitable energy descent. The edge set may be elegantly described and propagated by the level set approach of Osher and Sethian [61,62]. In [48] a level set based Newton-type regularized optimization algorithm has been derived for the minimization the original Mumford–Shah functional, which is the algorithmical basis for our method. For related approaches we refer to [20–22,48]. In particular, we consider Γ to be given as the zero level set of the level set function $v_\Gamma : \Omega \to \mathbb{R}$, i.e.,

$$\Gamma = \{x \,:\, v_\Gamma(x) = 0\}\,.$$

3.1 The reduced functional

The functional (4) depends on the variables $u_R, u_T, \boldsymbol{\phi}$ and Γ. In the process of minimization we may devise different strategies for the different variables. Fortunately the functional is quadratic in the variables u_R and u_T. Hence, we may minimize the energy for fixed Γ and $\boldsymbol{\phi}$ over image spaces of u_R and u_T. Let us now denote by $u_R[\Gamma]$ and $u_T[\Gamma, \boldsymbol{\phi}]$ the corresponding minimizers. They are obtained solving the Euler Lagrange equations with respect to u_R and u_T:

$$\begin{aligned} -\mu\Delta u_R + u_R &= u_{R,0} && \text{in } \Omega\backslash\Gamma \\ \partial_{n_\Gamma} u_R &= 0 && \text{on } \Gamma, \\ -\mu\Delta u_T + u_T &= u_{T,0} && \text{in } \Omega\backslash\Gamma^{\boldsymbol{\phi}}, \\ \partial_{n_{\Gamma^{\boldsymbol{\phi}}}} u_T &= 0 && \text{on } \Gamma^{\boldsymbol{\phi}}. \end{aligned} \tag{6}$$

It is obvious that the minimizer with respect to u_R depends only on Γ, whereas the minimizer with respect to u_T depends also on $\boldsymbol{\phi}$ via the domain of integration $\Omega\backslash\Gamma^{\boldsymbol{\phi}}$. Now we can define the *reduced* functional

$$\hat{E}[\Gamma, \boldsymbol{\phi}] = E[\Gamma, \boldsymbol{\phi}, u_R[\Gamma], u_T[\Gamma, \boldsymbol{\phi}]]. \tag{7}$$

To treat the optimization problem w.r.t. Γ which is given by the level set function v_Γ we make use of nowadays classical shape sensitivity calculus. For details we refer to the books of Sokołowski and Zolésio [66] or Delfour and Zolésio [33]. Furthermore, the Appendix of [48] gives a nice overview. For an energy $E[\Gamma] = \int_\Gamma \theta \, \mathrm{d}a$ depending on a domain boundary Γ we get

$$\langle \partial_\Gamma E[\Gamma]; \zeta \rangle = \int_\Gamma (\partial_{n_\Gamma}\theta + \theta h)\, \zeta \cdot n_\Gamma \, \mathrm{d}a \tag{8}$$

where Γ is supposed to be a $\mathscr{C}^1$-hypersurface, h is the mean curvature of Γ and ζ is a scalar perturbation of Γ in normal direction. Furthermore, for an energy $E[\Omega] = \int_\Omega \theta(\Omega, x)\, \mathrm{d}x$ depending on a domain Ω the shape derivative is given by

$$\langle \partial_\Gamma E[\Omega]; \zeta \rangle = \int_\Omega \theta'(\Omega; \zeta)\, \mathrm{d}x + \int_\Gamma \theta\, \zeta \, \mathrm{d}a, \tag{9}$$

where $\theta'(\Omega)$ is the shape derivative of the integrand θ with respect to a normal variation ζ of the domain boundary Γ extended to the whole domain. For details we refer to [36]. With these tools available, we are now able to derive the first variation of the reduced function $\hat{E}$ (7) with respect to the shape variable Γ and with respect to the deformation $\boldsymbol{\phi}$. Via a integral transform, we first decouple Γ and $\boldsymbol{\phi}$ and obtain

$$\begin{aligned} \hat{E}(\Gamma, \boldsymbol{\phi}) = {} & \frac{1}{2}\int_\Omega (u_R(\Gamma) - u_{R,0})^2 \, \mathrm{d}x \\ & + \frac{\mu}{2}\int_{\Omega\backslash\Gamma} \|\nabla u_R(\Gamma)\|^2 \, \mathrm{d}x \\ & + \frac{1}{2}\int_\Omega \left((u_T(\Gamma, \boldsymbol{\phi}) - u_{T,0})^2 \circ \boldsymbol{\phi} \right) |\det D\boldsymbol{\phi}| \, \mathrm{d}x \\ & + \frac{\mu}{2}\int_{\Omega\backslash\Gamma} \left(\|\nabla u_T(\Gamma, \boldsymbol{\phi})\|^2 \circ \boldsymbol{\phi} \right) |\det D\boldsymbol{\phi}| \, \mathrm{d}x \\ & + \nu \mathscr{H}^{d-1}(\Gamma) + \alpha E_{\mathrm{reg}}[\boldsymbol{\phi}]. \end{aligned}$$

Now we can apply (8) as well as (9), where we have to integrate along the boundaries from both sides of the contour, which leads to corresponding jump terms. We obtain

$$\begin{aligned} \left\langle \partial_\Gamma \hat{E}[\Gamma, \boldsymbol{\phi}]; \zeta \right\rangle = {} & \frac{1}{2}\int_\Gamma \Big([\![(u_R(\Gamma) - u_{R,0})^2]\!] \\ & + \mu [\![\|\nabla u_R(\Gamma)\|^2]\!] \Big)\, \zeta \, \mathrm{d}a \\ & + \frac{1}{2}\int_\Gamma \Big(\Big[\!\Big[(u_T(\Gamma, \boldsymbol{\phi}) - u_{T,0})^2 \Big]\!\Big] \\ & + \mu \Big[\!\Big[\|\nabla u_T(\Gamma, \boldsymbol{\phi})\|^2 \Big]\!\Big] \Big) \circ \boldsymbol{\phi} \, |\det D\boldsymbol{\phi}| \zeta \, \mathrm{d}a \\ & + \nu \int_\Gamma h\, \zeta \, \mathrm{d}a. \end{aligned} \tag{10}$$

Recall that $u_R[\Gamma]$ and $u_T[\Gamma, \boldsymbol{\phi}]$ are defined as the solutions of the corresponding elliptic boundary value problems (6). As described in [48], the terms involving the shape derivatives θ' disappear since they are derivatives of the energy w.r.t. u_R and u_T in direction of u_R' resp. u_T' and hence zero due to local optimality.

For the Gateaux derivative of $\hat{E}$ with respect to the deformation $\boldsymbol{\phi}$ in a direction $\boldsymbol{\psi}$ we obtain

$$\begin{aligned} \left\langle \partial_{\boldsymbol{\phi}} \hat{E}[\boldsymbol{\phi}]; \boldsymbol{\psi} \right\rangle = {} & \frac{1}{2}\int_{\Gamma^{\boldsymbol{\phi}}} \Big([\![|u_T(\Gamma, \boldsymbol{\phi}) - u_{T,0}|^2]\!] \\ & + \mu [\![|\nabla u_T(\Gamma, \boldsymbol{\phi})|^2]\!] \Big)\, (\boldsymbol{\psi} \circ \boldsymbol{\phi}^{-1} \cdot n_{\Gamma^{\boldsymbol{\phi}}}) \, \mathrm{d}a \\ & + \left\langle \partial_{\boldsymbol{\phi}} E_{\mathrm{reg}}[\boldsymbol{\phi}]; \boldsymbol{\psi} \right\rangle, \end{aligned} \tag{11}$$

where the transformed normal $n_{\Gamma^{\boldsymbol{\phi}}}$ is given by

$$n_{\Gamma^{\boldsymbol{\phi}}} = \frac{\mathrm{Cof}\, D\boldsymbol{\phi} n_\Gamma}{\|\mathrm{Cof}\, D\boldsymbol{\phi} n_\Gamma\|}.$$

3.2 Regularized gradient descent

The first variations contain jump terms of $u_T - u_{T,0}$ resp. $u_R - u_{R,0}$, for in general noisy initial data $u_{R,0}$ and $u_{T,0}$. Hence the regularity of the descent direction with respect to the L^2 metric is expected to be low. Thus, we will incorporate a regularized gradient descent (cf. [24,25]) with respect to both variables of the reduced functional $\hat{E}$.

As a metric on the space of deformation ϕ we consider

$$g_{\boldsymbol{\phi}}^\sigma(\boldsymbol{\psi}, \boldsymbol{\xi}) = \int_\Omega \boldsymbol{\psi} \cdot \boldsymbol{\xi} + \frac{\sigma^2}{2} \nabla\boldsymbol{\psi} : \nabla\boldsymbol{\xi},$$

where $A : B = \mathrm{tr}(A^T B)$. Let us remark that the inverse of the corresponding metric tensor is related to a Gaussian filtering of the deformation with filter width σ. Thus, the regularized descent direction $\boldsymbol{\psi}[\Gamma, \boldsymbol{\phi}]$ is given as a solution of the elliptic problem

$$g^{\sigma}_{\boldsymbol{\phi}}(\boldsymbol{\psi}[\Gamma, \boldsymbol{\phi}], \boldsymbol{\xi}) = -\left\langle \partial_{\boldsymbol{\phi}} \hat{E}[\Gamma, \boldsymbol{\phi}]; \boldsymbol{\xi} \right\rangle \tag{12}$$

for all variations $\boldsymbol{\psi}$ of $\boldsymbol{\phi}$.

Next, we discuss the regularization of the shape gradient with respect to the geometric variable Γ. We aim at finding a metric on normal variations of Γ, such that this resulting regularization is balanced with the regularized descent in the deformation. Hence, we ask for a suitable metric g^{σ}_{Γ} and defined a normal variation $\zeta[\Gamma, \boldsymbol{\phi}]$ on Γ as the regularized descent direction with respect to Γ by

$$g_{\Gamma}(\zeta[\Gamma, \boldsymbol{\phi}], \theta) = -\left\langle \partial_{\Gamma} \hat{E}[\Gamma, \boldsymbol{\phi}]; \theta \right\rangle. \tag{13}$$

An $H^{1,2}$ regular descent direction $d[\Gamma, \boldsymbol{\phi}]$ as we obtain it above, induces a motion of the transformed edge set $\Gamma^{\boldsymbol{\phi}}$ with a speed in normal direction which is given by $d \circ \boldsymbol{\phi}^{-1} n_{\Gamma^{\boldsymbol{\phi}}} \in H^{\frac{1}{2}}(\Gamma^{\boldsymbol{\phi}})$ for sufficiently regular $\Gamma^{\boldsymbol{\phi}}$. This motivates us to choose the shape gradient with respect to a suitable $H^{\frac{1}{2}}$-metric on Γ. By this choice we expect a reasonable balance between the regularization of update directions for the functional variable $\boldsymbol{\phi}$ and the geometric variable Γ. In order to define an inner product on $H^{\frac{1}{2}}(\Gamma)$ let us consider the boundary value problem

$$\begin{aligned} -\frac{\sigma^2}{2}\Delta\zeta + \zeta &= 0 \text{ in } \Omega, \\ \partial_{n_\Gamma}\zeta &= \eta \text{ on } \Gamma, \end{aligned} \tag{14}$$

for a some functional $\eta \in H^{-\frac{1}{2}}(\Gamma)$ given on Γ. Let us denote by $\mathcal{N} : H^{-\frac{1}{2}}(\Gamma) \to H^{\frac{1}{2}}(\Gamma)$ the linear operator representing the *Neumann-to-Dirichlet map* which maps η in (14) to the Dirichlet trace $\zeta|_{\Gamma}$ of the solution to (14). It is well known (cf.[52]) that $\mathcal{N}$ is an isomorphism. Finally, we define

$$g^{\sigma}_{\Gamma}(\zeta, \theta) := \left\langle \mathcal{N}^{-1}\zeta; \theta \right\rangle_{H^{-\frac{1}{2}}(\Gamma)\times H^{\frac{1}{2}}(\Gamma)}.$$

Thus, to evaluate the regularized shape gradient, we have to solve (14) with $\eta = \partial_{\Gamma}\hat{E}$ and to evaluate the trace of the solution on Γ.

3.3 A level set shape gradient descent method

In what follows let us describe how the optimization, that takes place over a shape and the deformation simultaneously, can be performed algorithmically. The topology of the solution Γ of the optimization problem is not known a priori. On the other hand, the gradient descent method depends on an initial guess. Level set methods provide a convenient framework for the representation and numerical evolution of sharp interfaces, especially when topological changes come into play. A detailed description of the Finite Element algorithm can be found in [36]. Here, we only briefly describe the key components in each step of the gradient descent:

- For given discrete deformation ϕ and level set function v the Finite Element solution for u_R and u_T in (6) on both sides of the interface is computed independently using Composite Finite Elements (cf. [45,64,72]). Thus, we avoid an explicit remeshing of the domains separated by the current level set of v representing the edge set Γ. Furthermore, it allows for an efficient multigrid solution of these elliptic problems, which leads to a significant speed-up of the algorithm. The transformation vector field $\boldsymbol{\phi}$ is discretized using standard Finite Elements.
- Once Finite Element approximations of u_R and u_T are known, the shape gradient and the gradient with respect to the deformation can be computed as Finite Element approximation on the domain Ω described by (13) and (12). Again two linear elliptic problems have to be solved to evaluate these regularized gradients.
- The gradient descent step in the deformation variable $\boldsymbol{\phi}$ is performed in a straightforward way.
- To evolve the level set function with a speed on the contour given by the discrete $\zeta[\Gamma, \boldsymbol{\phi}]$ on the discrete level set Γ, we consider an extension $\tilde{\zeta}$ onto a small neighborhood of the contour. Here, we have followed the widely used approach based on the solution of the transport equation

  $$\nabla\tilde{\zeta} \cdot \nabla d_{\Gamma} = 0 \quad \text{on} \quad \Omega \quad \text{and} \quad \tilde{\zeta} = \zeta[\Gamma, \boldsymbol{\phi}] \quad \text{on} \quad \Gamma,$$

  where d_{Γ} represents the signed distance function with respect to Γ (cf. [60,65]). To compute the discrete solution we used local numerical scheme proposed by Bornemann and Rasch [9].
- For the actual evolution of the level set function v via

  $$\partial_t v + \tilde{\zeta}\|\nabla v\| = 0 \quad \text{on} \quad \Omega \tag{15}$$

  we have applied a third-order accurate ENO-scheme (cf. [60]).

3.4 Numerical experiments

In Fig. 1 we have applied the algorithm to a pair of brain images. The top row shows a *proton density* weighted MR scan and a T1-weighted magnetic resonance image of the same patient. The initial misfit (bottom left) consists mainly of a shift and a small rotation. The algorithm finds the brain structure in both images well after about 250 steps. As desired, the resulting deformation represents mainly rigid

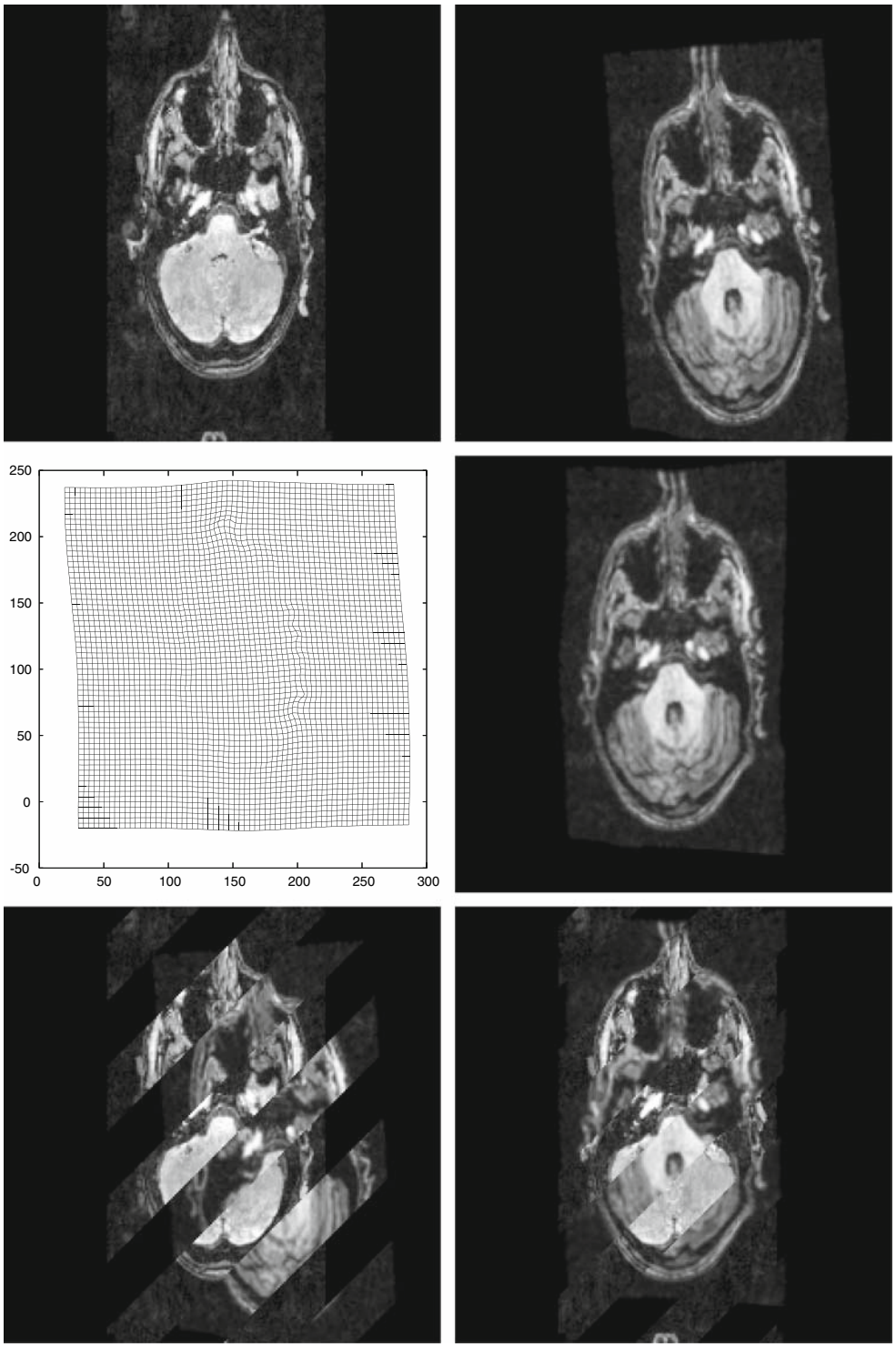

Fig. 1 Matching with the sharp interface Mumford–Shah model. *Top row* reference image u_R [proton density weighted MR-image (PD) of a human brain] an u_T (T1-weighted MR-image). *Middle row* deformation plot and the matching result $u_T \circ \phi$. *Bottom row* initial misfit shown as an striped overlaid reference and template compared to the final matching result. The parameters were chosen as $\mu = 200$, $\nu = 250$ and $\alpha = 5,000$. The iteration converged after 250 iterations

transformation between the images, enhanced by some minor local deformations (see Fig. 2 for the evolution of the interfaces Γ and $\phi(\Gamma)$).

Figure 3 demonstrates the competing effect of the regularization and the energy contributions which pull the contour towards the edges. We can exploit this in order to map an

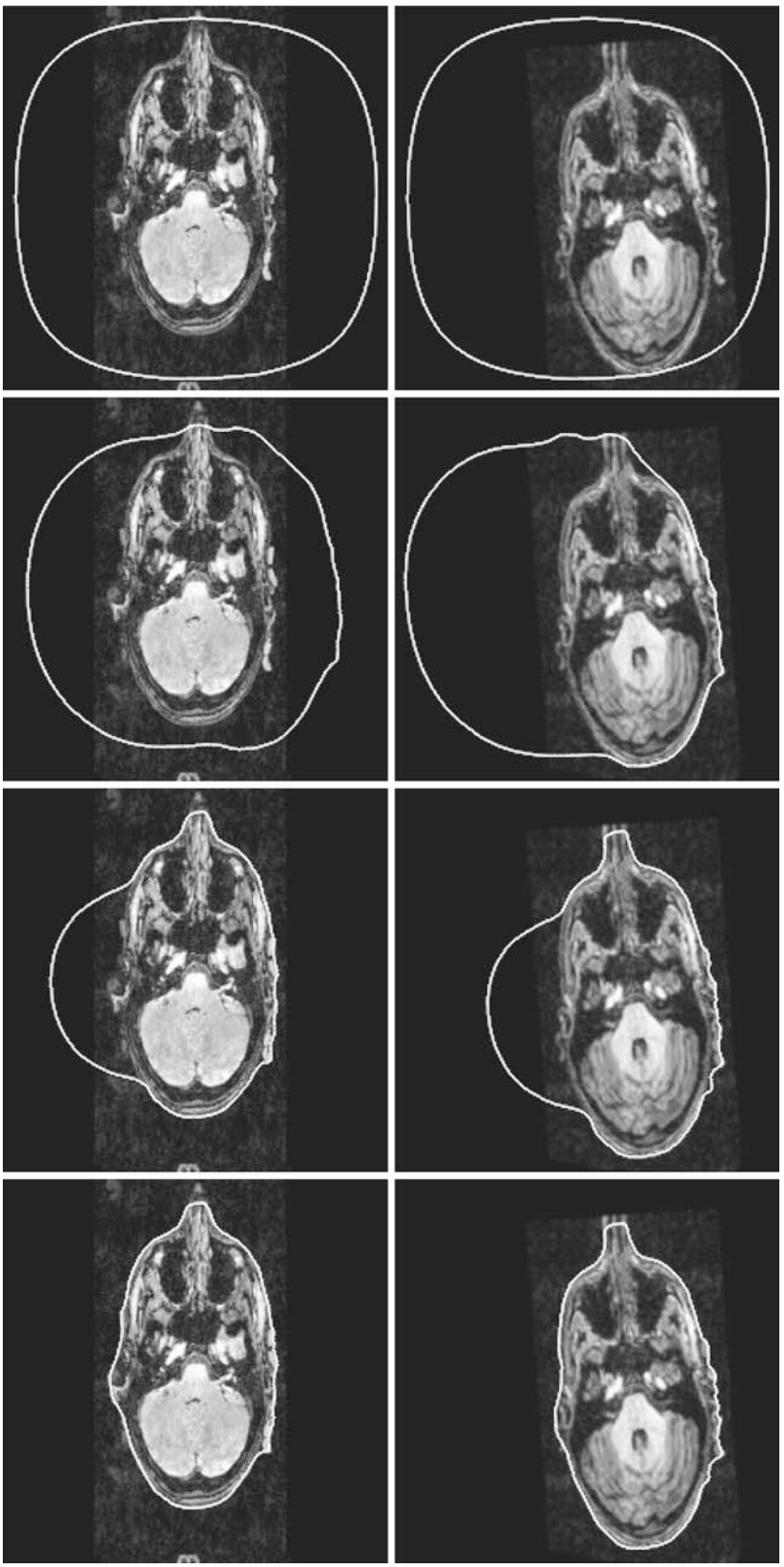

Fig. 2 Evolution of Γ in u_R in the *left column* and the evolution of $\phi(\Gamma)$ in u_T in the *right column* for iteration numbers 0, 50, 150 and 250 for the images and the problem setup as in Fig. 1

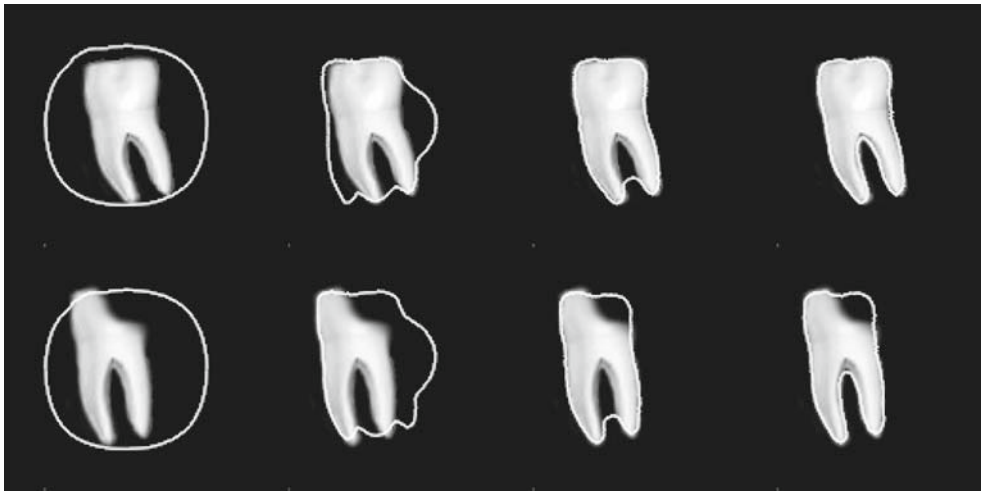

Fig. 3 Towards model-based reconstruction. The image at the *top left* shows an artificial reference model of a tooth. On the *bottom left* a nonlinearly deformed version of the reference with a large destroyed region is shown. Both images also show the initial contour Γ. The sequence shows the evolution of Γ and $\Gamma^{\boldsymbol{\phi}}$ for the iteration numbers 0, 20, 80, 320, where the parameters were chosen as $\mu = 50$, $\alpha = 200$ and $\nu = 5,000$

original reference shape (top row) to a given object, where the shape is partially corrupted (bottom row). Apart from the destroyed region the shapes differ also by a non-rigid deformation plus a translation. This can be observed well in the second column. At this stage, the regularization dominates and prohibits the contour in the bottom row to evolve towards the "visible" edge and prefers to adopt the contour from the reference image. This yields a reconstruction of the destroyed shape, which is optimal with respect to the regularization energy.

4 Phase-field approximation

Now, let us present an alternative to the previously described sharp interface model. In [5] Ambrosio and Tortorelli proposed a phase field approximation of the Mumford–Shah functional (1). Before we revise the approximation, we rewrite the Mumford–Shah energy to

$$F[u] = \int_{\Omega\setminus\Gamma} \|\nabla u\|^2 \,\mathrm{d}x + \frac{\mu}{2}\int_{\Omega} (u-u_0)^2 \,\mathrm{d}x + \nu\mathscr{H}^{d-1}(S_u)$$

defined on the space of piecewise $\mathscr{C}^1$ functions

$$PC^1(\Omega) = \left\{u \in L^\infty(\Omega)\right\}\left\{u \in \mathscr{C}^1(\Omega\setminus\overline{S_u}) \text{ and } \mathscr{H}^{d-1}(\overline{S_u}\cap\Omega\setminus S_u) = 0\right\}. \tag{16}$$

S_u denotes the complement of the set of Lebesgue points of u. Since PC^1 is not compact with respect to a suitable topology, the common approach (see [2,5,12,30,58] for further details) is to relax F to

$$\overline{F}(u) = \inf\left\{\liminf_{s\to\infty} F(u_s) : u_s \to u \in L^2(\Omega),\ u_s \in PC^1(\Omega)\right\}.$$

The Ambrosio–Tortorelli approximation results from a minimization of the functional

$$E_\epsilon[u,v] = \int_{\Omega}\left\{(u-u_0)^2 + \frac{\mu}{2}(v^2+k_\epsilon)\|\nabla u\|^2\right\}\mathrm{d}x + \nu\int_{\Omega}\left\{\epsilon\|\nabla v\|^2 + \frac{(1-v)^2}{4\epsilon}\right\}\mathrm{d}x$$

for fixed ϵ and $k_\epsilon > 0$. Here, v is a phase field variable which is supposed to be approximately 1 apart from the interface and approximate 0 on the edge set with a transition region of width 2ϵ. They have shown the Γ-convergence with respect to the strong L^2 topology of E_ϵ to the functional defined by $\overline{E}[u,v] = \overline{F}[u]$, iff $v \equiv 1$, and $\overline{E}[u,v] = +\infty$ otherwise.

Now, we suggest for the joint segmentation and registration problem an analogous coupled phase-field formulation by again introducing an auxiliary phase field variable v, describing the singularity set S_T of the image u_T, but at the same time $v\circ\boldsymbol{\phi}$ should energetically describe the edge set S_R in the image u_R. A corresponding energy formulation is then given by the minimization of

$$E^\epsilon_{\mathrm{AT}}[u_R,u_T,v,\boldsymbol{\phi}] := \frac{1}{2}\int_{\Omega}\left\{(u_R-u_{R,0})^2 + (u_T-u_{T,0})^2\right\}\mathrm{d}x$$

$$+\frac{\mu}{2}\int_\Omega \left\{(v^2\circ\boldsymbol{\phi}+k_\epsilon)\|\nabla u_R\|^2+(v^2+k_\epsilon)\|\nabla u_T\|^2\right\}\,\mathrm{d}x$$
$$+\frac{\nu}{2}\int_\Omega \left\{\epsilon\|\nabla v\|^2+\frac{1}{4\epsilon}(v-1)^2\right\}\,\mathrm{d}x \tag{17}$$

with $k_\epsilon = o(\epsilon)$. Here, the phase field function v corresponds to the contour $\Gamma^{\boldsymbol{\phi}}$ and the contour Γ is described by $v\circ\boldsymbol{\phi}$. The first integral measures the deviation of u_R and u_T to the data in the L^2-sense. The second integral now forces the signature v^2 to be small where u_T has steep gradients and, correspondingly, $v^2\circ\boldsymbol{\phi}$ to be small where u_R has steep gradients. On the other hand, this determines $\boldsymbol{\phi}$ to align the signature function in the reference domain to line up with the edges of u_R, and finally, for fixed signature and deformation, the smoothness of the images u_R and u_T is controlled, i. e., steep gradients of u_T are penalized where $v \not\approx 0$ and analogously for u_R.

Again, the deformation $\boldsymbol{\phi}$ will mainly be determined along the discontinuity sets. Indeed, as outlined above, away from the contours the phase field v will approximately be identical to 1, and hence variations of $\boldsymbol{\phi}$ will not change the energy in these regions. Hence, we again consider a nonlinear hyperelastic regularization given by the additional energy function $E_{\mathrm{reg}}[\phi]$ (2) and finally define

$$E^\epsilon[u_R,u_T,v,\boldsymbol{\phi}] := E^\epsilon_{\mathrm{AT}}[u_R,u_T,v,\boldsymbol{\phi}]+\alpha E_{\mathrm{reg}}[\boldsymbol{\phi}]$$

and ask for minimizers.

In contrast to the original approach of [4], where approximating elliptic but non-quadratic functionals have been used, the approximation of (17) gives rise to practicable numerical methodologies. We refer for instance to [7,63]. In order to discretize E^ϵ_{AT}, we follow the approach of Bourdin. In [10] he has proven the Γ-convergence of the discretized functionals against the functional $\overline{E}$. See also [11,19,34,40] for further details.

4.1 First variation of the energy

Let us first calculate the variations with respect to the variables u_R, u_T and v in directions ϑ, ξ, and ζ, respectively:

$$\begin{aligned}
&\left\langle \partial_{u_R} E^\epsilon_{\mathrm{AT}}[u_R,u_T,v,\boldsymbol{\phi}];\vartheta\right\rangle\\
&\quad=\int_\Omega (u_R-u_{R,0})\cdot\vartheta\,\mathrm{d}x\\
&\qquad+\mu\int_\Omega (v^2\circ\boldsymbol{\phi}+k_\epsilon)\nabla u_R\cdot\nabla\vartheta\,\mathrm{d}x\\
&\left\langle \partial_{u_T} E^\epsilon_{\mathrm{AT}}[u_R,u_T,v,\boldsymbol{\phi}];\xi\right\rangle\\
&\quad=\int_\Omega (u_T-u_{T,0})\cdot\xi\,\mathrm{d}x+\mu\int_\Omega (v^2+k_\epsilon)\nabla u_T\cdot\nabla\xi\,\mathrm{d}x\\
&\left\langle \partial_{v} E^\epsilon_{\mathrm{AT}}[u_R,u_T,v,\boldsymbol{\phi}];\zeta\right\rangle\\
&\quad=\mu\int_\Omega \|\nabla u_T\|^2 v\cdot\zeta\,\mathrm{d}x+\mu\int_\Omega \|\nabla u_R\|^2(v\circ\boldsymbol{\phi})\cdot(\zeta\circ\boldsymbol{\phi})\\
&\qquad+\nu\int_\Omega \epsilon\nabla v\cdot\nabla\zeta\,\mathrm{d}x+\nu\int_\Omega\frac{1}{4\epsilon}(v-1)\zeta\,\mathrm{d}x.
\end{aligned}\tag{18}$$

We rewrite (18) via the transformation formula:

$$\begin{aligned}
&\left\langle \partial_{v} E^\epsilon_{\mathrm{AT}}[u_R,u_T,v,\boldsymbol{\phi}];\zeta\right\rangle\\
&\quad=\mu\int_\Omega \|\nabla u_T\|^2 v\cdot\zeta\,\mathrm{d}x\\
&\qquad+\mu\int_\Omega \|\nabla u_R\|^2\circ\boldsymbol{\phi}^{-1} v\cdot\zeta\,\det D\boldsymbol{\phi}^{-1}\,\mathrm{d}x\\
&\qquad+\nu\int_\Omega \epsilon\nabla v\cdot\nabla\zeta\,\mathrm{d}x+\nu\int_\Omega\frac{1}{4\epsilon}(v-1)\zeta\,\mathrm{d}x.
\end{aligned}\tag{19}$$

Hence, for fixed v and $\boldsymbol{\phi}$ the reconstructed images u_R and u_T can be computed by solving the following elliptic problems

$$\begin{aligned}
u_R-\mu\mathrm{div}\left((v^2\circ\boldsymbol{\phi}+k_\epsilon)\nabla u_R\right) &= \mathcal{I}_h u_{R,0,\epsilon} \quad \text{in } \Omega,\\
\partial_\nu u_R &= 0 \quad \text{on } \partial\Omega
\end{aligned}\tag{20}$$

$$\begin{aligned}
u_T-\mu\mathrm{div}\left((v^2+k_\epsilon)\nabla u_T\right) &= \mathcal{I}_h u_{T,0,\epsilon} \quad \text{in } \Omega,\\
\partial_\nu u_T &= 0 \quad \text{on } \partial\Omega
\end{aligned}\tag{21}$$

where $\mathcal{I}_h$ denotes the interpolation operator. Since $v\geq 0$ the corresponding bilinear-forms are coercive. Furthermore, we are able to find for each u_T, u_R and $\boldsymbol{\phi}$ the optimal phase field v as the solution of the Euler–Lagrange equation with respect to the variation in the variable v, i.e.,

$$\begin{aligned}
&\mu\|\nabla u_T\|^2 v+\mu\|\nabla u_R\|^2\circ\boldsymbol{\phi}^{-1} v\,\det D\boldsymbol{\phi}^{-1}\\
&\quad+\frac{\nu}{4\epsilon}(v-1)-\nu\epsilon\Delta v=0 \quad \text{in } \Omega.
\end{aligned}\tag{22}$$

and $\partial_\nu v = 0$ on $\partial\Omega$. Finally, the variation of the energy with respect to the deformation in a direction ψ is given by

$$\begin{aligned}
&\left\langle \partial_{\boldsymbol{\phi}} E^\epsilon_{\mathrm{AT}}[u_R,u_T,v,\boldsymbol{\phi}];\psi\right\rangle\\
&\quad=\mu\int_\Omega \|\nabla u_R\|^2 v\circ\boldsymbol{\phi}\,(\nabla v\circ\boldsymbol{\phi}\cdot\psi)\,\mathrm{d}x\\
&\quad=\mu\int_\Omega \|\nabla u_R\|^2\circ\boldsymbol{\phi}^{-1} v\,(\nabla v\cdot\psi\circ\boldsymbol{\phi}^{-1})\,\det D\boldsymbol{\phi}^{-1}\,\mathrm{d}x.
\end{aligned}\tag{23}$$

Analogously to the approach chosen in the above sharp interface model, the energy functional can be reduced to depending only on $\boldsymbol{\phi}$, where $u_R[\boldsymbol{\phi}]$, $u_T[\boldsymbol{\phi}]$ and $v[\boldsymbol{\phi}]$ are determined as the unique solutions to the quadratic minimization problem for fixed $\boldsymbol{\phi}$:

$$\hat{E}^\epsilon[\boldsymbol{\phi}] = E^\epsilon[u_R[\boldsymbol{\phi}],u_T[\boldsymbol{\phi}],v[\boldsymbol{\phi}],\boldsymbol{\phi}]. \tag{24}$$

4.2 Multiscale gradient descent

Different to the sharp interface approach above the phase field approximation comes along with a natural scale parameter. As mentioned above the width of the diffusive interface turns out to be 2ϵ. On the same scale the images u_T and u_R are diffused close to edges of the initial images $u_{T,0}$ and $u_{R,0}$. Hence, the smoothness of energy variations will also depend on the scale parameter ϵ. On coarser scales we expect smoother descend directions and larger displacement can be rendered via the gradient descent. But, for decreasing ϵ one observed successively irregular variations. Indeed, the smoothness of $\partial_{\boldsymbol{\phi}} E^{\epsilon}_{AT}$ is controlled by the smoothness of $\boldsymbol{\phi}^{-1}$, u_R and v and the smoothness of v is steered directly by ϵ on account of the penalty term $\epsilon\|\nabla v\|^2$. Furthermore, for a small ϵ, v is close to 0 where $\|\nabla u_R\|^2 \circ \boldsymbol{\phi}^{-1}$ or $\|\nabla u_T\|^2$ are large and v is forced to be close to 1 in the rest of the domain on account of the amplified single well potential.

In summary, larger values of ϵ yield coarse and smooth approximations of the images, the phase field and the deformation. Hence, one starts with coarse approximations, to find a stationary point in the simplified energy landscape, iteratively reduces the approximation parameter ϵ by taking the solution of the previous scale as the new initial guess on the next finer scale.

Then on finer scales for small values of ϵ, the discrete descent direction tend to get irregular. Hence, it is again feasible to consider a regularized gradient descent and we consider the same regularized metric on variations of the deformation as in the sharp interface case.

On each scale the resulting Finite Element algorithm consists of a discrete gradient descent. Each gradient descent step can be decomposed as follows. For given $\boldsymbol{\phi}$ compute Composite Finite Element approximations for u_T, u_R and v as discrete solutions of (20), (21), and (22), respectively, and iterate these three solution steps until convergence. Then one proceeds by evaluating the descent direction w.r.t. the deformation and finally performs an update of the deformation $\boldsymbol{\phi}$ based on a line-search strategy.

Let us remark that on the finest scale ϵ has to be of the order of the grid size, since otherwise the transition zone of the phase field function cannot be resolved anymore by a Finite Element function.

4.3 Numerical experiments

In Fig. 4, we test the phase field algorithm with the same data as in the case of the sharp interface model. We observe very similar results. In fact, the phase field model seems to perform a better alignment in the interior of the skull. The phase field function captures edge details in the entire image, while the sharp interface framework focuses on the evolution of the predefined contour. This leads to a positive effect on the final alignment and to a slightly improved deformation. This can be seen very clearly in Fig. 5. It shows the phase field function at the initial stage and the final stage. Since, the coupled discontinuity problems aims at keeping the length of the interface short, the deformation will eventually try to map the edges in u_R onto the edges of u_T.

5 The main differences between the two approaches

The aim of this comparison of the level set and the phase field model is to illustrate and discuss the drawbacks and benefits of both approaches in this particular application of joint segmentation and registration. It naturally depends on the computational considerations, the conceptual framework and the specific application, which alternative will be the method of choice. In the following, we will point out some fundamental differences.

5.1 Methodological differences

Both, the level set approach and the phase field approach are famous for their topological flexibility. The process of splitting a curve into several curves is a smooth process in both frameworks and does not cause any conceptual problems.

The representations of the discontinuity set are fundamentally different in type. The level set method elegantly allows to represent, trace and evolve a given sharp interface. This fits well to the framework of the calculus of shape derivatives in which the current interface is given precisely. To be more precise, the level set method is just one way of evolving a sharp interface, in comparison to parametrizing the interface. We consider parametric versions as not competitive due to tremendous difficulties that arise at topology changes. For the sake of completeness, let us mention that one can also describe sharp interfaces by a phase field function by using suitable obstacle potentials. From the conceptional viewpoint of shape variation, those would then fall in the same category, since the motion would result from the shape variation of the shape functional. The Ambrosio–Tortorelli-approximation is however a diffuse representation. Instead of precisely representing the position of the interface, the phase-field function v only indicates the position of edges in a blurry way. This phase-field function has to be defined on the entire domain Ω and results directly from the solution of a simple elliptic PDE. The actual discontinuity set is then only given as minimizer $\Omega \to \{0, 1\}$ of the Γ-limit of sequence of approximation functionals for $\epsilon \to 0$. In actual computations however the phase field function has to be computed for ϵ of the order of the grid size. We conclude, that if the actual interface is of interest as the result of the algorithm, a sharp interface model, represented, e.g., by a level set function is favorable.

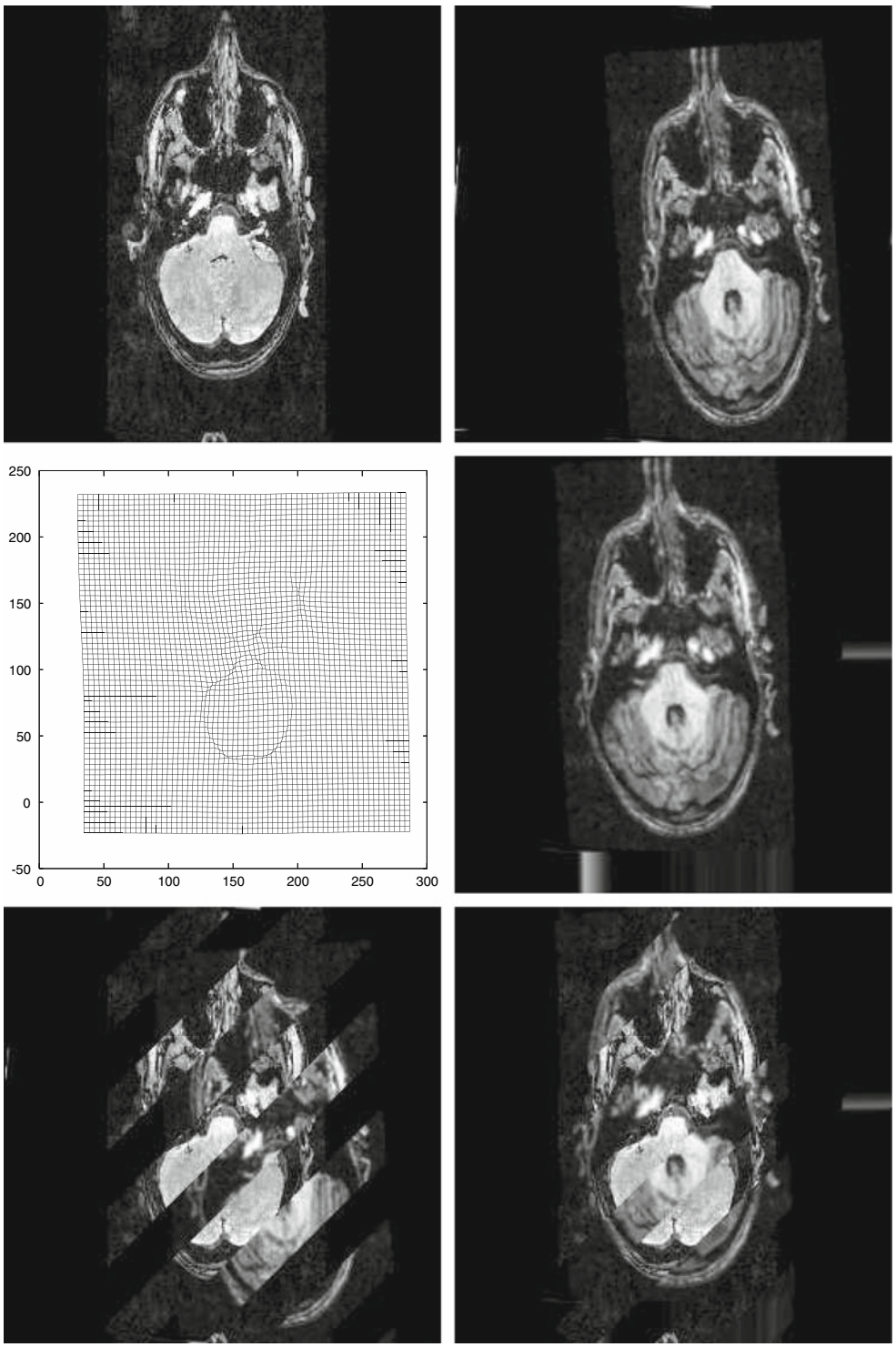

Fig. 4 Matching and results of the same problem set-up as in Fig. 1. *Top row* initial images u_R (PD) and u_T (T1). *Middle row* deformation plot and matching results $u_T \circ \phi$. *Bottom row* comparison of initial misfit and final matching result against the reference image

The classical level set framework is restricted to closed curves, and thus it does not allow to represent *crack tips* by a single level set function. Although this could be achieved by combining several level set functions with boolean operations, the phase field approach appears to be more flexible and practicable for the applications discussed here. The same is true for generating holes. The phase field representation is global by definition and respects the features of the images in the entire domain, with requiring any initialization. For sharp interface models, let us mention the concept of *topological*

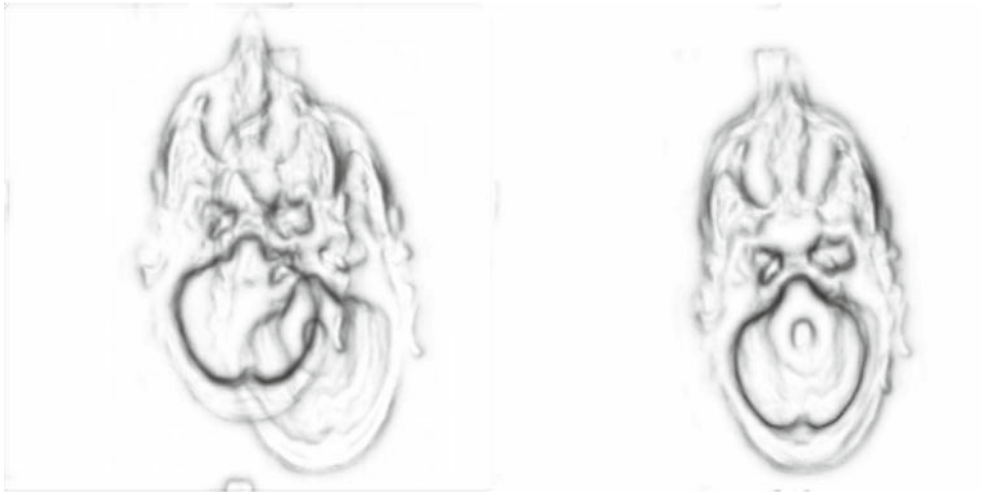

Fig. 5 Comparison of the phase-field function v after the first iteration (*left*) and after the final iteration (*right*)

derivatives [16]. By considering the limit for the change of the energy functional for arbitrary small holes, one can yield a descent of the functional with respect to topology. This is of great importance for example in structural mechanics. The sharp interface approach optimizes with respect to a given initial shape, while the phase field approach will try to align all dominant edges in the images simultaneously. In some cases however, when there are no counterparts of strong edges in the other image, the simultaneous matching of all features may be a counterproductive aim. The restriction to certain features only may be beneficial here.

The dependence on the initial condition in the case of the sharp interface model, does not necessarily mean to be a burden. Due to the non-convex structure of the joint discontinuity problem, the initial shape and position of the contour allows to give the user some kind of control over the matching process.

5.2 Computational considerations

Let us now compare the algorithmical effort related to both of the approaches. The phase field method can be set up in a straightforward way by solving elliptic and parabolic problems with coefficients which vary in space. Such problems are standard and can be solved with all PDE toolboxes. Due to the fact that the interface is represented by a smooth phase field function, the solution of the Helmholtz problems in the domains, which are divided by the free discontinuity is straightforward and does not require any additional effort to take care about free boundaries.

The sharp interface approach is more complicated to implement. The computation of the velocity requires to evaluate geometric entities and jumps of the traces of the functions u_R and u_T along the interface. In order to compute these functions, an algorithmical tool like Composite Finite Elements, a *Shortley-Weller* discretization or *Websplines* [49] has to be incorporated. In order to improve efficiency multigrid methods [44] have been applied. All this effort is honored by yielding the true derivative and thus the correct dynamics of the gradient flow. However, for the task of image registration, we are mainly interested in the minimization of the functional and not the evolution of the contour.

6 Conclusion

We have compared a level set based and a phase field model for simultaneous segmentation and registration of images by incorporating a Mumford–Shah type energy on the reference image as well as the template image, where the contour is transformed into the template image by a regularized deformation. The work is motivated by the fact, that, given an exact registration of two images of different modality, edge-extraction and segmentation can be enhanced considerably by combining complementary feature information from both modalities. On the other hand the process of registering a pair of images may rely on segmentations and feature-extractions of both images, which is often a very tedious process, especially if in some areas the feature information is very weak. Due to the coupling of the edge sets by the smooth deformation, the edge is driven to its correct shape.

Due to the regularization of the gradient flow, the minimization process has turned out to be stable and requires only a small number of iterations until convergence. On the other hand, the regularization and necessity of determining the solutions of the Helmholtz equations in the regions Ω_1 and Ω_2 requires the solution of elliptic PDEs.

The phase field method offers an interesting, convenient and efficient alternative to the level set approach if the main aim is registration and not segmentation. In contrast to the

level set function, the phase field parameter captures edge information in the entire domain. From an algorithmical point of view, the phase field method is certainly much easier to handle and only requires the solution of standard elliptical problems.

Both methodologies are very flexible and allow a wide range of extensions for model-based matching (introducing a priori knowledge into the functional as e.g. in [26,28]), optical flow estimation with discontinuities (see also [27]) and other areas.

Acknowledgments The authors thank PD Dr. Frithjof Kruggel from the MPI Neurosciences in Leipzig for kindly providing the medical images. The initial idea for this approach has emerged during the IPAM Workshop on Inverse Problems, September 2003. The project has been partially supported by the German Science Foundation in the priority programme SPP 1114 "Mathematical methods for time series analysis and digital image processing".

References

1. Alvarez, L., Snchez, J., Deriche, R., Weickert, J.: Dense disparity map estimation respecting image discontinuities: a pde and scale-space based approach. IAPR Workshop on Machine Vision no. 28–30, pp. 423–427 (2000)
2. Ambrosio, L., Faina, L., March, R.: Variational approximation of a second order free discontinuity problem in computer vision. SIAM J. Math. Anal. **32**(6), 1171–1197 (2001)
3. Ambrosio, L., Fusco, N., Pallara, D.: Functions of Bounded Variation And Free Discontinuity Problems. Oxford University Press, Oxford (2000)
4. Ambrosio, L., Tortorelli, V.M.: Approximation of functionals depending on jumps by elliptic functionals via Γ-convergence. Comm. Pure Appl. Math. **43**, 999–1036 (1990)
5. Ambrosio, L., Tortorelli, V.M.: On the approximation of free discontinuity problems. Boll. Un. Mat. Ital. B **6**(7), 105–123 (1992)
6. Ball, J.: Global invertibility of Sobolev functions and the interpenetration of matter. Proc. R. Soc. Edin. **88**, 315–328 (1988)
7. Belletini, G., Coscia, A.: Discrete approximation of a free discontinuity problem. Numer. Funct. Anal. Optim. **15**, 201–224 (1994)
8. Bonnet, A.: On the regularity of the edge set of Mumford–Shah minimizers. Prog. Nonlinear Diff. Equ. Appl. **25**, 93–103 (1996)
9. Bornemann, F., Rasch, C.: Finite-Element discretization of static Hamilton–Jacobi equations based on a local variation principle. (2004). See http://www.springerlink.com/content/v61q331816620gq1
10. Bourdin, B.: Image segmentation with a Finite Element method. ESIAM: Math. Modell. Numer. Anal. **33**(2), 229–244 (1999)
11. Bourdin, B., Chambolle, A.: Implementation of a Finite-Element approximation of the Mumford–Shah functional. Numer. Math. **85**(4), 609–646 (2000)
12. Braides, A.: Approximation Of Free Discontinuity Problems. Lecture Notes in Mathematics, vol. 1694. Springer, Heidelberg (1998)
13. Brook, A., Kimmel, R., Sochen, N.A.: Variation restoration and edge detection for color images. J. Math. Image Vis. **18**, 247–268 (2003)
14. Burger, M.: A framework for the construction of level set methods for shape optimization and reconstruction. Interfaces Free Bound. **5**, 301–329 (2003)
15. Burger, M.: Levenberg-Marquardt level set methods for inverse obstacle problems. Inv. Prob. **20**, 259–282 (2004)
16. Burger, M., Hackl, B., Ring, W.: Incorporating topological derivatives into level set methods. J. Comput. Phys. **194**, 344–362 (2004)
17. Caselles, V., Catté, F., Coll, T., Dibos, F.: A geometric model for active contours in image processing. Numer. Math. **66**, 1–31 (1993)
18. Caselles, V., Kimmel, R., Sapiro, G.: Geodesic active contours. Int. J. Comput. Vis. **22**(1), 61–79 (1997)
19. Chambolle, A.: Image segmentation by variatonal methods: Mumford–Shah functional and the discrete approximations. SIAM J. Appl. Math. **55**(3), 827–863 (1995)
20. Chan, T.F., Vese, L.A.: Image segmentation using level sets and the piecewise constant Mumford–Shah model. UCLA CAM Report 00–14, University of California, Los Angeles (2000)
21. Chan, T.F., Vese, L.A.: A level set algorithm for minimizing the Mumford–Shah functional in image processing. UCLA CAM Report 00–13, University of California, Los Angeles (2000)
22. Chan, T.F., Vese, L.A.: Active contours without edges. IEEE Trans. Image Process. **10**(2), 266–277 (2001)
23. Ciarlet, P.G.: Three-Dimensional Elasticity. Elsevier, New York (1988)
24. Clarenz, U., Droske, M., Rumpf, M.: Towards fast non-rigid registration. In: Inverse Problems, Image Analysis and Medical Imaging. AMS Special Session Interaction of Inverse Problems and Image Analysis, vol. 313, pp. 67–84. AMS, New York (2002)
25. Clarenz, U., Henn, S., Rumpf M., Witsch, K.: Relations between optimization and gradient flow methods with applications to image registration. In: Proceedings of the 18th GAMM Seminar Leipzig on Multigrid and Related Methods for Optimisation Problems, pp. 11–30 (2002)
26. Cremers, D., Kohlberger, T., Schnörr, C.: Nonlinear shape statistics in Mumford–Shah based segmentation. In: A. Heyden et al. (ed.) European Conference on Computer Vision (ECCV), Copenhagen, vol. 2351, pp. 93–108. Springer LNCS, Heidelberg (2002)
27. Cremers, D., Soatto, S.: Motion competition: a variational framework for piecewise parametric motion segmentation. Int. J. Comput. Vis. **62**(3), 249–265 (2005)
28. Cremers, D., Tischhäuser, F., Weickert, J., Schnörr, C.: Diffusion snakes: introducing statistical shape knowledge into the Mumford–Shah functional. Int. J. Comput. Vis. **50**(3), 1364–1379 (2002)
29. Dacorogna, B.: Direct Methods in the Calculus of Variations. Appl. Math. Sciences, vol. 78. Springer, Berlin (1989)
30. Dal Maso, G., Morel, J., Solimini, S.: A variational method in image segmentation: existence and approximation results. Acta Math. **168**, 89–151 (1996)
31. Davatzikos, C.A., Bryan, R.N., Prince, J.L.: Image registration based on boundary mapping. IEEE Trans. Med. Image **15**(1), 112–115 (1996)
32. De Giorgi, E., Carriero, M., Leaci, A.: Existence theorem for a minimum problem with free discontinuity set. Arch. Rat. Mech. Anal. **108**, 195–218 (1989)
33. Delfour, M.C., Zolésio, J.: Geometries and Shapes: Analysis, Differential Calculus and Optimization. Adv. Des. Control 4. SIAM, Philadelphia (2001)
34. Dibos, F., Séré: An approximation result for the minimizers of the Mumford–Shah functional. Boll. Un. Math. Ital. **11A**(1), (1997)
35. Droske, M.: On variational problems and gradient flows in image processing. Ph.D. thesis, Universität Duisburg-Essen (2005)
36. Droske, M., Ring, W.: A Mumford–Shah level-set approach for geometric image registration. SIAM J. Appl. Math. **66**(6), 2127–2148 (2006)
37. Droske, M., Rumpf, M.: Multi scale joint segmentation and registration of image morphology. IEEE Trans. Pattern Anal. Mach. Intell. **29**(12), 2181–2194 (2007)
38. Droske, M., Rumpf, M.: A variational approach to non-rigid morphological registration. SIAM Appl. Math. **64**(2), 668–687 (2004)

39. Evans, L.C., Gariepy, R.F.: Measure Theory and Fine Properties of Functions. CRC Press, Boca Raton (1992)
40. Feng, X., Prohl, A.: Analysis of gradient flow of a regularized Mumford–Shah functional for image segmentation and image inpainting. Math. Modell. Numer. Anal. (1999)
41. Féron, O., Mohammad-Djafari, A.: Image fusion and unsupervised joint segmentation using a hmm and mcmc algorithms. J. Electron. Image **14**(2) (2005)
42. Fried, M.: Image segmentation using adaptive finite elements. Technical Report, University of Canberra, Australia (2003)
43. Grenander, U., Miller, M.I.: Computational anatomy: an emerging discipline. Q. Appl. Math. **LVI**(4), 617–694 (1998)
44. Hackbusch, W.: Multigrid Methods and Applications. Springer, Berlin (1985)
45. Hackbusch, W., Sauter, S.: Composite finite elements for the approximation of pdes on domains with complicated microstructures. Numer. Math. **75**, 447–472 (1997)
46. Henn, S.: A Levenberg–Marquardt scheme for nonlinear image registration. BIT Numer. Math. **43**(4), 743–759 (2003)
47. Hintermüller, M., Ring, W.: A second order shape optimization approach for image segmentation. SIAM Appl. Math. **64**(2), 442–467 (2003)
48. Hintermüller, M., Ring, W.: An inexact Newton-cg-type active contour approach for the minimization of the Mumford–Shah functional. J. Math. Image Vis. **20**, 19–42 (2004)
49. Höllig, K., Reif, U., Wipper, J.: Weighted extended b-spline approximation of dirichlet problems. SIAM J. Numer. Anal. **39**(2), 442–462 (2001)
50. Joshi, S.C., Miller, M.I.: Landmark matching via large deformation diffeomorphisms. IEEE Trans. Med. Image **9**(8), 1357–1370 (2000)
51. Kapur, T., Yezzi, L., Zöllei, L.: A variational framework for joint segmentation and registration. IEEE CVPR-MMBIA (2001)
52. Kirsch, A.: An Introduction to the Mathematical Theory of Inverse Problems. Applied Mathematical Sciences, vol. 120. Springer, New York (1996)
53. Maes, F., Collignon, A., Vandermeulen, D., Marchal, G., Suetens, P.: Multi-modal volume registration by maximization of mutual information. IEEE Trans. Med. Image **16**(7), 187–198 (1997)
54. Mikula, K., Sarti, A., Sgallari, F.: Handbook of medical image analysis: segmentation and registration models. In: Suri, J. et al. (eds.) Co-volume level set method in subjective surface based medical image segmentation. Kluwer Academic/Plenum Publishers, New York (2004)
55. Miller, M., Trouve, A., Younes, L.: On the metrics and Euler–Lagrange equations of computational anatomy. Annu. Rev. Biomed. Eng. **4**, 375–405 (2002, in press)
56. Modersitzki, J., Fischer, B.: Fast diffusion registration. Special Issue of Contemporary Mathematics, AMS, New York (2000)
57. Modersitzki, J., Fischer, B.: Curvature based image registration. JMIV **18**(1) (2003)
58. Morel, J., Solimini, S.: Variational models in image segmentation. Birkäuser, Basel (1994)
59. Mumford, D., Shah, J.: Optimal approximation by piecewise smooth functions and associated variational problems. Comm. Pure Appl. Math. **42**, 577–685 (1989)
60. Osher, S.J., Fedkiw, R.P.: Level Set Methods and Dynamic Implicit Surfaces. Springer, Heidelberg (2002)
61. Osher, S.J., Paragios, N.: Geometric Level Set Methods in Imaging, Vision and Graphics. Springer, Heidelberg (2003)
62. Osher, S.J., Sethian, J.A.: Fronts propagating with curvature dependent speed: algorithms based on Hamilton–Jacobi formulations. J. Comput. Phys. **79**, 12–49 (1988)
63. Richardson, T.J., Mitter, S.K.: A variational formulation based edge focussing algorithm. Sadhana Acad. P. Eng. S. **22**(4), 553–574 (1997)
64. Sauter, S., Stahn, N.: Composite finite elements and multi-grid. part i: Convergence theory in 1-d. Technical Report, Preprint, 11-01, University of Zürich (2001)
65. Sethian, J.A.: Level Set Methods: Evolving Interfaces in Geometry, Fluid Mechanics, Computer Vision and Materials Sciences. Cambridge University Press, Cambridge (1996)
66. Sokołowski, J., Zolésio, J.P.: Introduction to shape optimization. In: Shape Sensitivity Analysis. Springer, Berlin (1992)
67. Thirion, J.P.: Image matching as a diffusion process: an analogy with maxwell's demon. Med. Image Anal. **2**, 243–260 (1998)
68. Tsai, A., Yezzi, A., Willsky, A.: Curve evolution implementation of the Mumford–Shah functional for image segmentation, denoising, interpolation, and magnification. IEEE Trans. Image Process. **10**(8), 1169–1186 (2001)
69. Unal, G., Slabaugh, G.: Coupled PDEs for non-rigid registration and segmentation. In: IEEE Computer Society International Conference on Computer Vision and Pattern Recognition (CVPR) (2005)
70. Vemuri, B., Ye, J., Chen, Y., Leonard, C.: Image registration via level-set motion: applications to atlas-based segmentation. Med. Image Anal. **7**, 1–20 (2003)
71. Viola, P.A., Wells III, W.: Alignment by maximization of mutual information. Technical Report. AITR-1548 (1995)
72. Warnke, R.: Schnelle Löser für elliptische Randwertprobleme mit springenden Koeffizienten. Dissertation, Zürich (2003)
73. Wells, W., Viola, P., Atsumi, H., Nakajima, S., Kikinis, R.: Multimodal volume registration by maximization of mutual information (1996)